Published in final edited form as:
Neuron. 2011 September 22; 71(6): 1102–1115. doi:10.1016/j.neuron.2011.08.008.

DPP6 establishes the A-type K+ current gradient critical for the regulation of dendritic excitability in CA1 hippocampal neurons

Wei Sun[1,2], **Jon K. Maffie**[3], **Lin Lin**[1], **Ronald S. Petralia**[4], **Bernardo Rudy**[3], and **Dax A. Hoffman**[1]

[1]Molecular Neurophysiology and Biophysics Unit, Eunice Kennedy Shriver National Institute of Child Health and Human Development, National Institutes of Health, Bethesda, MD

[2]Neuroscience Research Institute and Department of Neurobiology, Peking University Health Science Center, Beijing, China

[3]Dept. of Physiology and Neuroscience and Smilow Neuroscience Program, NYU School Medicine, New York, NY

[4]Laboratory of Neurochemistry, National Institute on Deafness and Other Communication Disorders, National Institutes of Health, Bethesda, MD

Summary

Subthreshold-activating A-type K^+ currents are essential for the proper functioning of the brain where they act to delay excitation and regulate firing frequency. In CA1 hippocampal pyramidal neuron dendrites, the density of A-type K^+ current increases with distance from the soma, playing an important role in synaptic integration and plasticity. The mechanism underlying this gradient has, however, remained elusive. Here, dendritic recordings from mice lacking the Kv4 transmembrane auxiliary subunit DPP6 revealed that this protein is critical for generating the A-current gradient. Loss of DPP6 led to a decrease in A-type current, specifically in distal dendrites. Decreased current density was accompanied by a depolarizing shift in the voltage-dependence of channel activation. Together these changes resulted in hyperexcitable dendrites with enhanced dendritic AP back-propagation, calcium electrogenesis and induction of synaptic long-term potentiation. Despite enhanced dendritic excitability, firing behavior evoked by somatic current injection was mainly unaffected in DPP6-KO recordings, indicating compartmentalized regulation of neuronal excitability.

Introduction

Voltage-gated potassium (Kv) channels play important roles in regulating the excitability of neurons and other excitable cells. Subthreshold activating, rapidly inactivating, A-type K^+ currents are non-uniformly expressed in the primary apical dendrites of rat hippocampal CA1 pyramidal neurons, with density increasing with distance from the soma (Hoffman et al., 1997). Adding to their impact, the kinetics and voltage dependence of A-type currents change as a function of distance from the soma such that their probability of opening is enhanced in distal compared to proximal dendrites. Increased density and activation of A-

Address correspondence to: Dax A. Hoffman, 35 Lincoln Drive, MSC 3715, Building 35, Room 3C-905, Bethesda, MD 20892-3715; hoffmand@mail.nih.gov.

type K^+ channels together act to dampen dendritic excitability, notably by limiting the back-propagation of action potentials (bAPs) into distal dendrites. Dendrites express voltage-gated Na^+ channels at a uniform density (Magee and Johnston, 1995), and regulate back-propagation via K^+-channel activity suggesting a physiological role for gated dendritic AP back-propagation. Consistent with this hypothesis, dendritic APs have been shown to have important roles in synaptic integration and plasticity (Spruston, 2008).

Although several types of K^+ channel pore-forming subunits produce A-type K^+ currents, including members of the Kv1, Kv3, and Kv4 subfamilies, results from a number of different experimental approaches have suggested that members of the Kv4 subfamily are the main determinants of the somatodendritic A-type K^+ current (Chen et al., 2006; Kim et al., 2005; Nerbonne et al., 2008). There are three Kv4 genes, two of which, Kv4.2 and Kv4.3, are prominently expressed in brain (Serodio and Rudy, 1998). However, of these two, CA1 neurons express only Kv4.2 (Maletic-Savatic et al., 1995; Menegola et al., 2008; Rhodes et al., 1995; Serodio and Rudy, 1998). Furthermore, Kv4.2 has been shown to a key constituent of the A-type K^+ current in CA1 dendrites which, in addition to controlling dendritic excitability, is targeted for modulation during synaptic plasticity (reviewed in Kim and Hoffman, 2008). Consistent with the conclusion that A-type K^+ channels in CA1 dendrites are composed of Kv4.2 pore forming subunits, deletion of the Kv4.2 gene results in a specific, uncompensated loss of A-type K^+ currents from CA1 apical dendrites, leading to an increase of bAP amplitude (Chen et al., 2006). However, the firing properties of CA1 pyramidal cells are only slightly altered after genetic loss of Kv4.2, due to an upregulation of non-Kv4 subunits, most likely Kv1 family members, in the somatic region of CA1 neurons along with increased GABAergic conductances (Andrásfalvy et al., 2008; Chen et al., 2006).

Kv4.2 expression and properties are potently regulated by auxiliary subunits as well as via phosphorylation (reviewed in Jerng et al., 2004; Maffie and Rudy, 2008; Shah et al., 2010). The DPP6 auxiliary subunit protein, which is expressed in CA1 neurons, has recently been identified in genomic screens from some populations as an Autism Spectrum Disorder (Marshall et al., 2008; Noor et al., 2010) and ALS susceptibility gene (Cronin et al., 2008; van Es et al., 2008). DPP6 enhances the opening probability and single channel conductance of Kv4 channels and increases channel surface expression in heterologous systems (Kaulin et al., 2009; Maffie and Rudy, 2008; Nadal et al., 2003). A ternary complex of Kv4, DPP6 and Kv channel interacting proteins (KChIPs) are thought to underlie the native A-type K^+ current in CA1 neurons (Kim and Hoffman, 2008; Maffie and Rudy, 2008).

To investigate the influence of DPP6 in a native system we generated conditional DPP6 knockout mice (DPP6fl/fl). These mice were crossed to a Cre deleter strain expressing Cre recombinase in the germline to generate DPP6 null alleles (DPP6-KO mice). In patch clamp recordings from wild type (WT) mouse CA1 hippocampal dendrites, we observed that the density of A-type currents increased with distance from the soma, as found previously for rats (Hoffman et al., 1997). However, in dendritic recordings from DPP6-KO mice, the A-current distribution in CA1 primary apical dendrites was altered so that the density was, on average, the same throughout the primary apical dendrite. Accordingly, dendritic excitability was enhanced in CA1 dendrites from acute hippocampal slices prepared from adult DPP6-KO mice: bAPs were better able to invade distal dendrites, trains of APs were more faithfully conveyed than in recordings from WT mice, and the threshold frequency for the generation of Ca^{2+} spikes and long-term potentiation (LTP) was lowered in DPP6-KO dendrites. In contrast to the critical role of DPP6 in dendritic excitability, firing behavior evoked by somatic current injections was only minorly affected in DPP6-KO CA1 recordings. In addition to establishing a role for DPP6 in generating the A-current gradient in CA1 neurons, these observations provide evidence that the enhanced dendritic A-current

is particularly important for the regulation of dendritic excitability including dendritic spiking and plasticity.

Results

Creation and characterization of DPP6-KO mice

We have previously shown using siRNA that acute knockdown of DPP6 moderately influences the firing patterns of hippocampal CA1 neurons in somatic recordings from hippocampal organotypic slice cultures (Kim et al., 2008). However it is at the distal apical dendrites of CA1 neurons that A-current expression and activation prominently control excitability and the small caliber of dendrites in cultured neurons precludes electrophysiological recordings from distal sites. Therefore, to investigate the functional significance of DPP6 in mature dendrites, we generated conditional DPP6 knockout mice (DPP6-KO, Figure 1A). DPP6-KO mice displayed a total loss of DPP6 mRNA and protein (Figure 1B–D). The closely related family member DPP10 is not normally expressed in CA1 pyramidal dendrites (Zagha et al., 2005) and is not upregulated in these cells in DPP6-KO mice (Figure 1E).

DPP6-KO mice lack a dendritic A-type K^+ current gradient

To investigate the effect of DPP6 loss on A-type K^+ currents in CA1 dendrites, we mapped K^+ channel densities with dendritic patch clamp recordings (Figure 2A,B). In CA1 dendrites, the total outward current consists of transient, A-type K^+ currents along with slower/non-inactivating, sustained K^+ currents. These two components can be isolated using a voltage prepulse inactivation protocol (Experimental Procedures). In rats, the transient current increases with distance from the soma in CA1 apical dendrites (Hoffman et al., 1997). This gradient was also found in outside-out patch recordings from CA1 dendrites of WT mice (Figure 2A). However, loss of DPP6 altered the transient current distribution in CA1 primary apical dendrites such that density is, on average, the same throughout the primary apical dendrite (Figure 2A). The average transient current amplitude in recordings from distal dendrites (220–240 μm) from DPP6-KO mice is the same as found in DPP6-KO proximal dendrites (<40 μm, ~12 pA in both WT and DPP6 recordings). Transient current density was similar for the two groups until >80 μm after which amplitudes increased in WT but not DPP6-KO recordings ($p<0.01$). No difference in average sustained K^+ current amplitude was found between the WT and DPP6-KO ($p>0.1$, Figure 2A), which had similar amplitudes throughout the primary apical dendrite. Dendritic, cell-attached recordings showed an even more dramatic increase in distal A-current density in WT compared to DPP6-KO dendrites, with no observed change in sustained current density (Figure 2B).

Western blot analyses of proteins expressed in tissue microdissected from the CA1 somatic and distal dendritic regions supported these results, showing a specific decrease in distal dendritic Kv4.2 expression. In tissue from somatic region of DPP6-KO slices, total Kv4.2 was not significantly changed from WT (1.00±0.04, $p>0.05$, Figure 2C). However, tissue extracted from distal dendrites showed a decrease in Kv4.2 protein expression in DPP6-KO mice compared to WT (0.69±0.05 normalized to WT, $p<0.05$, Figure 2D). DPP6 antibodies produce no labeling in DPP6-KO mice (Figure 1D) and no reactivity with the antibody was detected in immunoblots of microdissected DPP6-KO tissue (data not shown).

A decrease of dendritic Kv4.2 was also observed in immunohistochemical staining experiments performed in slices from DPP6-KO mice compared to WT ($p<0.05$, Figure 2E,F) while synaptic and extrasynaptic Kv4.2 expression, as determined by immunogold labeling, were significantly reduced in electron micrographs of spines in DPP6-KO mice (Figure 2G). DPP6 has been shown to enhance surface expression of Kv4 channels in

heterologous expression systems (Nadal et al., 2003; Seikel and Trimmer, 2009) but had not been previously shown to regulate subcellular targeting and, therefore, channel distributions in neurons. Together, these data indicate that DPP6 is necessary for the generation of the functional A-type K^+ current gradient observed in CA1 neurons. The loss of the A-current gradient is consistent with our results showing less Kv4.2 expression in distal dendrites and spines of DPP6-KO neurons.

Another possible interpretation of our findings is that, given the loss of Kv4.2 protein in DPP6-KO dendrites, Kv4.2 channels are replaced by another A-type K^+ channel, which is not expressed in a gradient. In fact, Kv4.2-KO mice exhibit a compensatory upregulation of channels, presumably of the Kv1 subfamily (Chen et al., 2006). We therefore investigated if other A-type K^+ channels are upregulated in the dendrites of DPP6-KO mice and if the properties of the A-type K^+ currents in the knockouts are consistent with being mediated by Kv4.2 proteins.

The A-type K^+ channels remaining in DPP6-KO dendrites are Kv4-mediated

We first investigated whether there is increased expression of other subunits capable of forming A-type K^+ currents in hippocampal tissue from DPP6-KO mice. Western blot analyses showed that the expression levels of Kv1.1, Kv1.4, Kv3.4 or Kv4.3 proteins did not differ between WT and DPP6-KO hippocampal homogenates (Figure 3A–D). Nor did we find any differences in tissue microdissected from the CA1 somatic and distal dendritic fields for these proteins data not shown). We also investigated the properties of the A-currents in DPP6-KO mice. The A-currents remaining in DPP6-KO proximal and distal dendrites exhibited a pharmacological profile similar to WT and consistent with Kv4.2 but not Kv1 channels, showing little sensitivity to low concentrations of 4-AP (Figure 3E–H). TEA at 1 mM blocked about 33% of the transient current in both WT and DPP6-KO, similar to that previously found in rat dendrites (Hoffman et al., 1997).

Recovery from inactivation is quite different for Kv4 channels as compared to the A-type K^+ channels formed by other pore-forming subunits (Coetzee et al., 1999). Kv4 channels recover from inactivation much faster than Kv1 or Kv3 channels even in the absence of KChIPs or DPPs, both of which further accelerate inactivation recovery. Figure 4A shows that A-type K^+ currents measured in at −100 mV in WT proximal and distal dendrites displayed rapid recovery from inactivation. Recovery from inactivation in recordings from DPP6-KO dendrites, however, was demonstrably slower than that of WT controls (τ_{recov}=12.43 ± 0.46 ms for WT, n=10; τ_{recov}=184.54 ± 9.32 ms for DPP6-KO, n=9, p<0.05). This change is consistent with the effects of DPP6 on inactivation recovery of Kv4 currents in heterologous cells (Maffie and Rudy, 2008; Nadal et al., 2003). However, these time constants are still too fast for the A-current to be mediated by Kv1 or Kv3 channels, which take seconds to recover from inactivation (Coetzee et al., 1999).

Although these data on recovery from inactivation suggest Kv4-mediated currents remain in DPP6-KO dendrites, what explains the dramatically faster recovery in proximal vs. distal dendrites? One possibility is a difference in KChIP auxiliary subunit expression remaining in dendrites of DPP6-KO neurons, which share the ability to accelerate recovery from inactivation with DPP subunits in heterologous systems (Jerng et al., 2005). Previous studies found that Kv4.2 deletion induced a virtual elimination of KChIP expression suggesting that the expression level of Kv4 and KChIP proteins are tightly coupled (Chen et al., 2006; Menegola and Trimmer, 2006). Of the four known KChIP isoforms (KChIP1–4), the two prominently expressed in the CA1 are KChIP2 and KChIP4 (Rhodes et al., 2004). As expected we found little expression of KChIP1 or KChIP3 in punched hippocampal tissues (data not shown). Similar to our results for Kv4.2 protein expression (Figure 2C,D), we found the total KChIP2 protein expression level to be equivalent in the somatic area of WT

and DPP6-KO slices (total KChIP2 in DPP6-KO=1.04 ± 0.04 normalized to WT, n=3, p<0.01, Figure 4C,D) but significantly reduced in the distal dendrites of DPP6-KO slices compared to WT (total KChIP2 in DPP6-KO=0.57 ± 0.12 normalized to WT, n=3, p<0.01, Figure 4C,D). Analysis using a pan-KChIP antibody showed a significant decrease in two bands (Figure 4C), perhaps indicating concurrent reduction of KChIP4 proteins in distal dendrites.

Other properties of the A-currents in the dendrites were also consistent with these being mediated by Kv4 channels in the absence of DPP6. In recordings from rat CA1 distal dendrites, A-channels exhibit a hyperpolarized activation curve compared to that found in the soma and proximal dendrites (Hoffman et al., 1997). Recordings from WT mice showed a similar activation curve shift (Figure 4E,F; $V_{1/2}$=−16 and −28 mV for proximal and distal dendrites, respectively, p<0.05). This distal hyperpolarization of the activation curve was not found in dendritic recordings from DPP6-KO mice where the proximal and distal channels exhibited nearly identical activation curves (Figure 4E,F; $V_{1/2}$=−11 and −8 mV for proximal dendrites and distal dendrites, respectively, p>0.1). Dendritic A-currents were also found to be slower to inactivate in DPP6-KO recordings compared to WT (Figure 4G,H). These changes are consistent with the strong influence of DPP6 on the voltage-dependence of Kv4 activation and inactivation rates observed in heterologous expression systems and, along with our results above, suggest that DPP6 prominently impacts A-currents in distal dendrites.

In contrast to the activation curve results above, there was no difference in steady-state inactivation between proximal and distal dendrites in WT control recordings ($V_{1/2}$=−78, k=−12 for proximal <40 μm, n=10; $V_{1/2}$ =−77 mV, k=−12, for distal dendrites 160 μm, n=14, data not shown). However, consistent with results from heterologous expression studies (Amarillo et al., 2008; Jerng et al., 2005; Nadal et al., 2003), loss of DPP6 produced a depolarizing-shift in the inactivation curve in proximal dendritic recordings compared to wild type ($V_{1/2}$=−69, k=−10, n=17, p<0.05), slightly increasing the fraction of channels available for activation from a given holding potential. Steady-state inactivation was similarly depolarized in distal dendrites ($V_{1/2}$=−68mV, k=−10, n=16).

In sum, our characterization of A-currents remaining in DPP6-KO dendritic recordings suggests a population of Kv4 channels that have lost DPP6 modulation. Because KChIP subunits prominently act to accelerate recovery from inactivation, it seems likely that at least a portion of the remaining Kv4 channels are in complex with KChIP2, and possibly KChIP4 subunits. The difference in recovery rates between proximal (faster recovery) and distal dendrites (slower recovery) suggests the possibility that the expression of these Kv4-KChIP complexes may be more prominent in the proximal dendrites in DPP6-KO CA1 neurons (see Discussion).

DPP6-KO CA1 pyramidal neuron apical dendrites are hyperexcitable

Lack of an activation curve shift, along with the decrease in current density for DPP6 distal dendrites, both act to substantially decrease the amount of transient current expected to be activated at a given membrane potential in DPP6-KO dendrites compared to WT controls. To investigate DPP6 influences on dendritic excitability in hippocampal CA1 neurons, we performed current clamp experiments in dendritic whole-cell recordings. In dendritic recordings from DPP6-KO mice, APs initiated via antidromic stimulation were better able to invade distal dendrites compared to WT (Figure 5A). Significant differences in bAP amplitude began at distances more than 100 μm from the soma, similar to the location where differences in A-current density between WT and DPP6-KO mice were observed (Figure 5A). As an estimate of Na^+ channel density, we measured the maximal rate of rise of APs in WT and DPP6-KO mice (Figure 5D,E). Finding no differences between the groups, and

given that AP amplitude is predominately dependent on the permeability ratio of Na^+ and K^+ ions (Colbert et al., 1997), we conclude that DPP6 regulates AP back-propagation into CA1 dendrites by enhancing A-type K^+ channel expression and regulating their properties to enhance channel open probability.

In CA1 neurons, AP back-propagation decreases with activity (Spruston et al., 1995) due to a combination of slow recovery from inactivation for dendritic Na^+ channels and the activity of A-type K^+ channels (Colbert et al., 1997; Jung et al., 1997). To investigate activity-dependent AP back-propagation in DPP6-KO mice, trains of bAPs were evoked at three stimulus frequencies, 10Hz, 20Hz, and 50Hz, by antidromic stimulation and recorded ~160 μm from the soma. In each of these trains, bAP amplitude progressively decreased in WT recordings such that the 10^{th} AP amplitude was only 50–60% that of the first (Figure 5B,C). However, DPP6-KOrecordings showed a remarkable decrease in the amount of attenuation, particularly at the lower frequencies. As expected, AP maximal rise dv/dt decreased during the bAP trains similarly in WT and DPP6-KO recordings as Na^+ channels enter an inactivated state (Figure 5E).

Frequency dependent AP back-propagation is functionally critical in the generation of Ca^{2+} spikes and burst firing in pyramidal neurons (Larkum et al., 1999). The ‘critical frequency' is the frequency of bAP trains where a dendritic Ca^{2+} spike is induced. Here, critical frequency was measured using dual whole-cell current-clamp recordings from the soma and apical dendrites in CA1 WT and DPP6-KO neurons by inducing trains of five APs with somatic current injection at frequencies ranging from 20 Hz to 200 Hz (Figure 6A). WT dendrites had a critical frequency of 127.8 ± 4.9 Hz (Figure 6B–D, n=9). DPP6-KO dendrites were significantly more excitable with an average critical frequency of 85.0 ± 5.7 Hz (Figure 6B–D, n=8, p<0.05).

We have observed previously that this type of complex firing is critical for the induction of LTP using a theta burst pairing protocol (Hoffman et al., 2002). Using a similar protocol (Figure 7A), we found that the spike-timing window for LTP induction is extended in recordings from DPP6-KO CA1 neurons compared to WT (Figure 7B–E). A theta burst protocol, consisting of two APs delivered 31–35 ms after synaptic stimulation to induce 5 EPSPs at 100 Hz, led to LTP in both WT and DPP6-KO recordings (Figure 7B,E). When the APs were delivered 41–45 ms after the onset of synaptic stimulation, however, synaptic potentiation was only observed in DPP6-KO recordings (Figure 7D,E). APs delayed greater that 46 ms relative to synaptic stimulation failed to induce LTP in either group (Figure 7E). We found that LTP induction in both WT and DPP6-KO recordings was coincident with enhanced depolarization via putative Ca^{2+} spikes supporting the notion that burst firing enhances LTP induction (Figure 7F–G).

Despite the considerable effect on dendritic excitability and synaptic plasticity, elimination of DPP6 had only minor affects on firing behavior evoked by somatic current into CA1 neurons (Figure 8A–E). No change was observed for the number of APs evoked by a 200 pA current injection (Figure 8C), first AP onset time (Figure 8D), or threshold potential in CA1 pyramidal neurons (Figure 8E). However, compared with WT, we did find a significant difference in the AHP in DPP6-KO (Figure 8F). The enhanced AHP in DPP6-KO recordings may be due to slower A-current inactivation during repolarization (Figure 4G,H).

These relatively minor changes in excitability measured in the soma compared to with that found in dendrites are reminiscent of those found for CA1 pyramidal cells after genetic loss of Kv4.2. However, in Kv4.2-KO mice, this was due to an upregulation of non-Kv4 subunits, most likely Kv1 family members, in the somatic region of CA1 neurons along with increased GABAergic conductances (Andrásfalvy et al., 2008; Chen et al., 2006). In DPP6-

KO, we do not find evidence for upregulation of other Kv subunits (Figures 3,4), nor are there any significant changes in tonic GABA currents or mIPSCs (Figure 8G–J). These differences between Kv4.2-KO and DPP6-KO mice lead to the suggestion that somatic excitability (e.g. AP threshold, onset time, number) but not the excitability of distal primary apical dendrites is under compensatory homeostatic control.

Discussion

We found that genetic loss of DPP6 eliminates the enhanced expression of A-type K^+ currents in the distal apical dendrites of mouse hippocampal CA1 pyramidal neurons. The channels remaining in DPP6-KO dendritic recordings were less responsive than WT, prominently displaying more depolarized activation and slower recovery from inactivation. Together with the decrease in total current, these properties sum to severely decrease the impact of A-currents on excitability in distal DPP6-KO dendrites. DPP6-KO dendrites exhibited enhanced propagation of single APs and less frequency dependent attenuation during AP trains. Enhanced bAP propagation resulted in a decrease in the frequency of APs needed to induce Ca^{2+} spikes and, consequently, enhanced LTP induction in DPP6-KO recordings. These findings have global implications for synaptic plasticity and integration in dendrites as back-propagating AP amplitude affects the amount of depolarization and Ca^{2+} influx experienced by synapses at different locations and by the same synapse during repetitive firing observed during learning (Colbert et al., 1997; Jung et al., 1997; Remy et al., 2009; Spruston et al., 1995). In addition, these results indicate that DPP6-KO mice may prove useful in future studies aimed at discerning the physiological function of activity-dependent dendritic AP propagation.

Impact of DPP6 on A-type K^+ channels expressed in distal dendrites

Studies in heterologous systems have shown that DPP6 has a number of critical effects that promote Kv4 channel function. In addition to its effects on activation and inactivation, it enhances membrane expression, increases single channel conductance and accelerates recovery from inactivation (Kaulin et al., 2009; Maffie and Rudy, 2008; Nadal et al., 2003). Our results suggest that these functions are particularly relevant for distal CA1 dendrites. How then are DPP6-Kv4 complexes targeted to distal dendrites? The presence of DPP6 auxiliary subunits may enrich Kv4 expression in distal dendrites, either through selective transporting or membrane retention. The structure of the DPP6 protein (predominately extracellular with a single transmembrane domain) hints at a possible role for an extracellular anchoring partner. This partner could be expressed in glia, as part of the extracellular matrix, or presynaptically and could be organized in a proximal to distal gradient. A related DPP family member, DPP4, has previously been shown to associate with the extracellular matrix (Hanski et al., 1988).

Given that spine density increases with distance from the soma (Megias et al., 2001), could the increased A-current found in distal dendrites represent a pool of spine localized, DPP6-containing Kv4 channels? Addressing this possibility using EM, we found that Kv4.2 immunogold puncta were decreased but not absent from spines (Figure 2G). This result suggests that DPP6 is not specifically required to target Kv4.2 to spines but may still indicate that co-assembly with DPP6 stabilizes Kv4.2 expression. We note also that, despite the apparent augmented effects of DPP6 in distal dendrites, DPP6 does appear to still have a role in regulating channels expressed proximally, as recordings in DPP6-KO slices showed these channels to have slightly more depolarized activation, steady-state inactivation and slower inactivation than in their WT counterparts. Together these lines of evidence point toward enhanced but not exclusive expression and/or retention of DPP6-containing channels in distal dendrites. Further studies investigating the subcellular assembly and trafficking of Kv4-DPP6 proteins in a native setting are required to fully describe the molecular

mechanisms underlying the specialized effect of DPP6 on A-current expression in distal dendrites.

In a previous study, the voltage-dependence of distal dendritic A-channel activation was found to be hyperpolarized compared to those found in the soma and proximal dendrites (Hoffman et al., 1997). Activation of PKA or PKC (likely acting through MAPK) shifted the curve back toward levels found in the proximal dendrites (Hoffman and Johnston, 1998; Yuan et al., 2002). A simple explanation for this result would be if dendrites contain a kinase/phosphatase gradient. However, the loss of the distance-dependent voltage-dependence to activation in DPP6-KO dendrites shows that DPP6 is also critically involved. Potentially, DPP6 could facilitate phosphorylation or other post-translational processes that are necessary for the dendritic expression profile. A promising avenue for future study would be to investigate whether DPP6-containing complexes represent a more mobile pool that is permissive for activity-dependent trafficking. Activity-dependent trafficking requires an intact PKA phosphorylation site (S552) on the Kv4.2 C-terminus (Hammond et al., 2008) and a recent study has found that both DPP6 and KChIP subunits confer sensitivity to PKA modulation in heterologous cells (Seikel and Trimmer, 2009).

In addition to deceased Kv4.2 expression in distal dendrites of DPP6-KO mice, we found less expression of KChIP proteins, another class of Kv4 auxiliary subunits. Given the results of previous studies that found that Kv4.2 deletion induced a virtual elimination of KChIP expression, suggesting that the expression levels of Kv4 and KChIP proteins are tightly coupled (Chen et al., 2006; Menegola and Trimmer, 2006), it seems likely that the decrease of Kv4.2 expression we found in DPP6-KO dendrites (Figure 2C–G) is the primary cause of the KChIP2 decrease shown in Figure 4C,D. However, we do see a difference in the rate of recovery from inactivation between proximal (faster recovery) and distal dendrites (slower recovery) (Figure 4A,B). This could indicate a KChIP subunit gradient in dendrites with a greater proportion of KChIP-associated Kv4 channels in proximal dendrites than in the distal dendrites. On the other hand, KChIP co-expression with Kv4 subunits in heterologous systems has been shown to have numerous effects on channel properties in addition to accelerating recovery from inactivation, which do not suggest a KChIP gradient. Notably, KChIP co-expression results in channels which inactivate more slowly than currents generated by Kv4 subunits expressed alone (An et al., 2000), or those in Kv4-DPP6 complexes (Amarillo et al., 2008; Jerng et al., 2005). However, while DPP6-KO displayed slower inactivation than WT, the difference in inactivation rates between proximal and distal dendrites (Figure 4G,H) is not as extreme as the differences we observed for recovery from inactivation (Figure 4A,B). Clearly, the situation *in vivo* is more complex than in expression systems and even more so in KO mice. More research is necessary to determine the presence of additional accessory and/or post-translational modifications to the channels, which could alter their properties in neurons, and to uncover the dendritic expression profile of various KChIP subunits.

DPP6 specifically affects dendritic excitability

In contrast to the explicit effect of DPP6 on dendritic AP propagation and Ca^{2+} spike initiation; intrinsic excitability measured in the soma was only mildly affected in recordings from CA1 DPP6-KO neurons. Firing profiles measured upon somatic current injection were basically indiscernible between WT and DPP6-KO with the exception of a slightly enhanced AHP in KO neurons (Figure 8). In a previous study on Kv4.2-KO mice, AP firing was also relatively normal despite enhanced AP back-propagation and altered distance-dependent mEPSC amplitude profiles (Andrásfalvy et al., 2008). In Kv4.2-KO mice, the preserved membrane excitability and firing patterns are likely the result of compensatory up-regulation of another K^+ channel subunit, possibly of the Kv1 family (Chen et al., 2006) in addition to increased GABAergic input (Andrásfalvy et al., 2008). However, our biochemical (Figure

4A–D), pharmacological (Figure 4E–H), and electrophysiological data (Figure 3G,H), all indicate that DPP6-KO CA1 neurons do not undergo any molecular compensation aimed at rescuing any of the dendritic phenotypes. In addition we found no compensatory regulation of GABA-mediated phasic or tonic currents (Figure 8).

Together the data from Kv4.2-KO and DPP6-KO mice suggest that somatic excitability (e.g. AP threshold, onset time, number of APs) but not the excitability of distal primary apical dendrites is under compensatory homeostatic control. What is the nature of this privileged perisomatic over dendritic compensation? One plausible scenario would be if the mechanisms responsible for this type of homeostasis of membrane excitability were triggered in response to changes in perisomatic changes in excitability. In this case, the cell does not monitor dendritic excitability, suggesting a sensor that is localized near the soma. A good candidate for the messenger would be Ca^{2+} influx during AP repolarization, which displays a relatively constant amplitude and duration in the soma compared to dendrites. Alternatively, due to their location distant from the nucleus, dendritic channels and receptors may simply be untethered from strict homeostatic excitability mechanisms. In any event it is surprising that dendritic excitability is not more closely regulated. Dendritic voltage-gated ion channels regulate the processing and storage of incoming information in CA1 pyramidal neurons (Shah et al., 2010). Perhaps the dynamic nature of channel properties and expression during normal function in dendrites prohibits the establishment of a set point state of excitability. We should make the distinction that the applicable data comes only from recordings in CA1 primary apical dendrites. Oblique dendrites may well employ mechanisms to homeostatically regulate their excitability.

In CA1 neurons, AP back-propagation decreases with activity (Spruston et al., 1995) due to a combination of slow recovery from inactivation for dendritic Na^+ channels and the activity of A-type K^+ channels (Colbert et al., 1997; Jung et al., 1997). We found DPP6 to be particularly important in the regulation of back-propagation at lower frequencies (Figure 5B,C). An explanation would be that normally a certain fraction of A-type K^+ channels are able to recover from inactivation in between APs but that without DPP6, the remaining A-type channels are too slow to recover from inactivation, allowing greater back-propagation. DPP6 therefore may be an important contributor to the cellular and circuit level mechanisms of theta rhythm (5–10 Hz) found in EEG recordings of the hippocampus during exploratory behavior and REM in the hippocampus.

In addition to enhanced back-propagation, we observed that Ca^{2+} spikes were more readily generated in DPP6-KO dendrites. The activation of dendritic voltage-gated Ca^{2+} channels by back-propagating APs results at a “critical” frequency will induce a burst of mixed Ca^{2+} and Na^+ action potentials in CA1 pyramidal neurons. Dendritic voltage-gated K^+ channels modulate this change in AP firing mode from single to burst firing (Golding et al., 1999; Magee and Carruth, 1999). We found that the critical frequency for Ca^{2+} electrogenesis in WT neurons of around 130 Hz was dramatically lowered to only 85 Hz in DPP6-KO neurons. We have observed previously that this type of complex firing is critical for the induction of GluA1-independent long-term potentiation (LTP) of synaptic inputs using a theta burst pairing protocol (Hoffman et al., 2002). Using a similar protocol, it has been shown that Kv4.2-KO mice have a lower threshold for LTP induction than WT (Chen et al., 2006; Zhao et al., 2010). Accordingly, we report here that the spike-timing window for LTP induction enhanced in DPP6-KO CA1 neurons (Figure 7). DPP6, by strengthening and accelerating A-channel activity in distal apical dendrites, acts to limit the time window during which coincident bAP and synaptic depolarization initiates burst firing, consisting of mixed Ca^{2+} and Na^+ spikes, which facilitates LTP induction.

DPP6, dendritic integration and neurological disease

The functional impact of the increase in dendritic excitability, burst firing and associated mistiming in plasticity induction in DPP6-KO mice remain to be determined, however there are expected to be behavioral consequences. Dendritic integration of synaptic inputs is fundamental to information processing in neurons of diverse function, serving as a link between synaptic molecular pathways and higher-order network function. Dendritic ion channels play a critical role in regulating information flow in dendrites and are targets for modulation during synaptic plasticity (Shah et al., 2010). The importance of ion channels in this process is highlighted by evidence from a recent *in vivo* study suggesting that neuronal output involves the summation of distributed inputs from multiple dendrites (Jia et al., 2010). Normal experience-dependent changes in the excitability of dendrites (dendritic plasticity), involving the downregulation of A-type K^+ currents, may represent a mechanism by which neurons store recent experience in individual dendritic branches (Makara et al., 2009). Mislocated or improper regulation of A-type K^+ currents will therefore greatly impact dendritic function, propagating errors to network and behavioral levels. We show here that DPP6, with its large extracellular domain and distinctive effects on Kv4 channels in distal dendrites is critical to normal dendritic function. Plasticity of dendritic branch excitability may also involve DPP6 if forthcoming studies conclude that DPP6 affects the activity-dependent trafficking of Kv4 channels. Future studies will also investigate the effect of DPP6 in synaptic development and behavior. Intriguingly, a number of genome-wide studies of neurological diseases have implicated DPP6 as a potential susceptibility gene in Autism Spectrum Disorder, Schizophrenia and ADHD (Cronin et al., 2008; Marshall et al., 2008; van Es et al., 2008). Dendritic excitability may turnout to be a common function affected by these neurological diseases.

Experimental Procedures

PCRs, in Situ Hybridization, Immunhistochemistry and Electron microscopy

These procedures were performed using standard, published techniques. Expanded protocols for these experiments are presented as Supplemental Material. Briefly, PCR genotyping was performed using standard methods with primers DPP6F1 5'-TCGCTCTTGGCAGTCTGAA-3' and DPP6B1 5´-AATAGTATCATGAAATCCAGAACC-3' to yield PCR products of 377 bp for WT and 135 bp for KO alleles. Quantitative PCR studies were performed with a 384-well configuration ABI 7900 SDS system using Power SYBR-Green PCR Master Mix (Applied Biosystems). Each cDNA sample, equivalent to RNA from one whole brain of WT and KO mice, was run in triplicate for the target. Digoxigenin labeled antisense DPP10 riboprobes were prepared using constructs produced by PCR cloning of DPP10 cDNA, accession number AY557199, with primers GGAAATACGAAATGACATCTGACACCTGG and GAGGCATACAACTTCATGTCTGAGATGGG to amplify a 982-bp. Nonradioactive *in situ* hybridization was conducted as described previously (Zagha et al., 2005). Immunohistochemical studies were performed as previously described (Zagha et al., 2008). Slices were blocked and incubated in primary antibody directed against Kv4.2 (NeuroMab) and DPP6 (Clark et al., 2008). Immunolabeling was visualized using the appropriate CY3 conjugated secondary antibody (Jackson Laboratories). Immunogold analysis was carried out as described previously (Petralia et al., 2010). A random sample of micrographs from the CA1 stratum radiatum of the hippocampus was taken and analyzed, from 2 experiments, with 3+3 and 2+2 WT+KO mice, respectively; the 2 experiments produced similar results and the data were combined (total 646 WT and 642 KO spine profiles).

Microdissection experiments

A dissection stage was frozen on dry ice plus 70% ethanol and placed under a dissection microscope, surrounded by TRIS buffered saline or Optimal Cutting Temperature solution. Eight hippocampal slices (300 μm thick) from each 6–8 week old C57BL/6 WT (B6) and DPP6-KO mouse brain were removed from the cutting chamber and frozen immediately on the miscrodissection platform. CA1 somatic and dendritic areas were microdissected using a small neuro-punch tool (internal diameter 0.31mm, Fine Science Tools). Punched CA1 tissue was collected in lysis buffer and stored on ice until assayed.

Punched CA1 tissue extruded from mouse brain slices was lysed in lysis buffer (150 mM NaCl, 20 mM Tris-HCl, 1% NP40, 0.5% SDS) and protease inhibitor mixture (Roche), and incubated for 20 min on ice, then sonicated 5 times for 5 seconds each. The lysate was centrifuged at 15,000 × g for 20 min at 4°C, and the protein concentration of the supernatant was measured by the BCA assay (Pierce Biotechnology). Equal amounts of protein were separated by electrophoresis on 10% SDS poly-acrylamide gels (Invitrogen) and transferred to nitrocellulose membranes. The separated proteins were immuonoblotted using Kv4.2 (1:2000, NeuroMab) or GAPDH (1: 5000, Calbiochem) antibody and visualized by Alexa Fluor 680 secondary antibody (1:10,000, Invitrogen) and Alexa Fluor 800 secondary antibody (1:10,000, Rockland). Immunoreactivity was detected with the Odyssey infrared imaging system (LI-COR Biosciences). Quantification of results was performed using Odyssey software (LI-COR Biosciences).

Slice preparation and electrophysiology

Hippocampal slices (250 μm thick) were prepared from 6- to 8-week-old male B6 WT and DPP6-KO mice, according to methods approved by The National Institute of Child Health and Human Development's Animal Care and Use Committee. Standard slice preparation and recording techniques were used. Expanded protocols for these experiments including solution contents are presented as Supplemental Material. Statistical significance of recording data was evaluated using Student's t-test (unpaired, two tails). *p* values are reported in the text or in the figure legends with values less than 0.05 considered significant. All recordings were analyzed using Clampfit 10.1 (Molecular Devices), Microsoft Excel, Minianalysis (Synaptosoft) and/or IGOR Pro (WaveMetrics).

HIGHLIGHTS

- Mice were created lacking the autism-associated Kv4 auxiliary subunit gene, DPP6.
- DPP6-KO mice lack the normal hippocampal dendritic A-type K^+ current gradient.
- Enhanced voltage-dependent A-channel activation in dendrites is lost in DPP6-KO.
- DPP6-KO dendrites but not somata are hyperexcitable.
- Synaptic plasticity is more readily induced in DPP6-KO mice.

Supplementary Material

Refer to Web version on PubMed Central for supplementary material.

Acknowledgments

This work was supported by the NICHD and NIDCD Intramural Research Programs and by NINDS grant NS045217 (BR). We thank Dr. Ya-Xian Wang for help with the immunogold study and Begum Choudhury for excellent technical assistance.

References

Amarillo Y, De Santiago-Castillo JA, Dougherty K, Maffie J, Kwon E, Covarrubias M, Rudy B. Ternary Kv4.2 channels recapitulate voltage-dependent inactivation kinetics of A-type K+ channels in cerebellar granule neurons. J Physiol. 2008; 586:2093–2106. [PubMed: 18276729]

An WF, Bowlby MR, Betty M, Cao J, Ling HP, Mendoza G, Hinson JW, Mattsson KI, Strassle BW, Trimmer JS, Rhodes KJ. Modulation of A-type potassium channels by a family of calcium sensors. Nature. 2000; 403:553–556. [PubMed: 10676964]

Andrásfalvy BK, Makara JK, Johnston D, Magee J. Altered synaptic and non-synaptic properties of CA1 pyramidal neurons in Kv4.2 KO mice. The Journal of Physiology. 2008

Chen X, Yuan L, Zhao C, Birnbaum S, Frick A, Jung W, Schwarz T, Sweatt J, Johnston D. Deletion of Kv4.2 Gene Eliminates Dendritic A-Type K+ Current and Enhances Induction of Long-Term Potentiation in Hippocampal CA1 Pyramidal Neurons. Journal of Neuroscience. 2006; 26:12143–12151. [PubMed: 17122039]

Clark BD, Kwon E, Maffie J, Jeong HY, Nadal M, Strop P, Rudy B. DPP6 Localization in Brain Supports Function as a Kv4 Channel Associated Protein. Front Mol Neurosci. 2008; 1:8. [PubMed: 18978958]

Coetzee WA, Amarillo Y, Chiu J, Chow A, Lau D, McCormack T, Moreno H, Nadal MS, Ozaita A, Pountney D, et al. Molecular diversity of K+ channels. Ann N Y Acad Sci. 1999; 868:233–285. [PubMed: 10414301]

Colbert CM, Magee JC, Hoffman DA, Johnston D. Slow recovery from inactivation of Na+ channels underlies the activity-dependent attenuation of dendritic action potentials in hippocampal CA1 pyramidal neurons. J Neurosci. 1997; 17:6512–6521. [PubMed: 9254663]

Cronin S, Berger S, Ding J, Schymick JC, Washecka N, Hernandez DG, Greenway MJ, Bradley DG, Traynor BJ, Hardiman O. A genome-wide association study of sporadic ALS in a homogenous Irish population. Hum Mol Genet. 2008; 17:768–774. [PubMed: 18057069]

Golding NL, Jung HY, Mickus T, Spruston N. Dendritic calcium spike initiation and repolarization are controlled by distinct potassium channel subtypes in CA1 pyramidal neurons. J Neurosci. 1999; 19:8789–8798. [PubMed: 10516298]

Hammond RS, Lin L, Sidorov MS, Wikenheiser AM, Hoffman DA. Protein kinase a mediates activity-dependent Kv4.2 channel trafficking. J Neurosci. 2008; 28:7513–7519. [PubMed: 18650329]

Hanski C, Huhle T, Gossrau R, Reutter W. Direct evidence for the binding of rat liver DPP IV to collagen in vitro. Exp Cell Res. 1988; 178:64–72. [PubMed: 2900773]

Hoffman DA, Johnston D. Downregulation of transient K+ channels in dendrites of hippocampal CA1 pyramidal neurons by activation of PKA and PKC. J Neurosci. 1998; 18:3521–3528. [PubMed: 9570783]

Hoffman DA, Magee JC, Colbert CM, Johnston D. K+ channel regulation of signal propagation in dendrites of hippocampal pyramidal neurons. Nature. 1997; 387:869–875. [PubMed: 9202119]

Hoffman DA, Sprengel R, Sakmann B. Molecular dissection of hippocampal theta-burst pairing potentiation. Proc Natl Acad Sci U S A. 2002; 99:7740–7745. [PubMed: 12032353]

Jerng HH, Kunjilwar K, Pfaffinger PJ. Multiprotein assembly of Kv4.2, KChIP3 and DPP10 produces ternary channel complexes with ISA-like properties. J Physiol. 2005; 568:767–788. [PubMed: 16123112]

Jerng HH, Pfaffinger PJ, Covarrubias M. Molecular physiology and modulation of somatodendritic A-type potassium channels. Mol Cell Neurosci. 2004; 27:343–369. [PubMed: 15555915]

Jia H, Rochefort NL, Chen X, Konnerth A. Dendritic organization of sensory input to cortical neurons in vivo. Nature. 2010; 464:1307–1312. [PubMed: 20428163]

Jung HY, Mickus T, Spruston N. Prolonged sodium channel inactivation contributes to dendritic action potential attenuation in hippocampal pyramidal neurons. J Neurosci. 1997; 17:6639–6646. [PubMed: 9254676]

Kaulin YA, De Santiago-Castillo JA, Rocha CA, Nadal MS, Rudy B, Covarrubias M. The dipeptidyl-peptidase-like protein DPP6 determines the unitary conductance of neuronal Kv4.2 channels. J Neurosci. 2009; 29:3242–3251. [PubMed: 19279261]

Kim J, Hoffman DA. Potassium channels: newly found players in synaptic plasticity. Neuroscientist. 2008; 14:276–286. [PubMed: 18413784]

Kim J, Nadal MS, Clemens AM, Baron M, Jung SC, Misumi Y, Rudy B, Hoffman DA. Kv4 accessory protein DPPX (DPP6) is a critical regulator of membrane excitability in hippocampal CA1 pyramidal neurons. J Neurophysiol. 2008; 100:1835–1847. [PubMed: 18667548]

Kim J, Wei DS, Hoffman DA. Kv4 potassium channel subunits control action potential repolarization and frequency-dependent broadening in rat hippocampal CA1 pyramidal neurones. J Physiol. 2005; 569:41–57. [PubMed: 16141270]

Larkum ME, Kaiser KM, Sakmann B. Calcium electrogenesis in distal apical dendrites of layer 5 pyramidal cells at a critical frequency of back-propagating action potentials. Proc Natl Acad Sci U S A. 1999; 96:14600–14604. [PubMed: 10588751]

Maffie J, Rudy B. Weighing the evidence for a ternary protein complex mediating A-type K+ currents in neurons. J Physiol. 2008; 586:5609–5623. [PubMed: 18845608]

Magee JC, Carruth M. Dendritic voltage-gated ion channels regulate the action potential firing mode of hippocampal CA1 pyramidal neurons. J Neurophysiol. 1999; 82:1895–1901. [PubMed: 10515978]

Magee JC, Johnston D. Characterization of single voltage-gated Na+ and Ca2+ channels in apical dendrites of rat CA1 pyramidal neurons. J Physiol. 1995; 487(Pt 1):67–90. [PubMed: 7473260]

Makara JK, Losonczy A, Wen Q, Magee JC. Experience-dependent compartmentalized dendritic plasticity in rat hippocampal CA1 pyramidal neurons. Nat Neurosci. 2009; 12:1485–1487. [PubMed: 19898470]

Maletic-Savatic M, Lenn NJ, Trimmer JS. Differential spatiotemporal expression of K+ channel polypeptides in rat hippocampal neurons developing in situ and in vitro. J Neurosci. 1995; 15:3840–3851. [PubMed: 7751950]

Marshall CR, Noor A, Vincent JB, Lionel AC, Feuk L, Skaug J, Shago M, Moessner R, Pinto D, Ren Y, et al. Structural variation of chromosomes in autism spectrum disorder. American journal of human genetics. 2008; 82:477–488. [PubMed: 18252227]

Megias M, Emri Z, Freund TF, Gulyas AI. Total number and distribution of inhibitory and excitatory synapses on hippocampal CA1 pyramidal cells. Neuroscience. 2001; 102:527–540. [PubMed: 11226691]

Menegola M, Misonou H, Vacher H, Trimmer JS. Dendritic A-type potassium channel subunit expression in CA1 hippocampal interneurons. Neuroscience. 2008; 154:953–964. [PubMed: 18495361]

Menegola M, Trimmer JS. Unanticipated region- and cell-specific downregulation of individual KChIP auxiliary subunit isotypes in Kv4.2 knock-out mouse brain. J Neurosci. 2006; 26:12137–12142. [PubMed: 17122038]

Nadal MS, Ozaita A, Amarillo Y, Vega-Saenz de Miera E, Ma Y, Mo W, Goldberg EM, Misumi Y, Ikehara Y, Neubert TA, Rudy B. The CD26-related dipeptidyl aminopeptidase-like protein DPPX is a critical component of neuronal A-type K+ channels. Neuron. 2003; 37:449–461. [PubMed: 12575952]

Nerbonne J, Gerber B, Norris A, Burkhalter A. Electrical remodelling maintains firing properties in cortical pyramidal neurons lacking KCND2-encoded A-type K+ currents. The Journal of Physiology. 2008; 586:1565–1579. [PubMed: 18187474]

Noor A, Whibley A, Marshall CR, Gianakopoulos PJ, Piton A, Carson AR, Orlic-Milacic M, Lionel AC, Sato D, Pinto D, et al. Disruption at the PTCHD1 Locus on Xp22.11 in Autism spectrum disorder and intellectual disability. Sci Transl Med. 2010; 2 49ra68.

Petralia RS, Wang YX, Hua F, Yi Z, Zhou A, Ge L, Stephenson FA, Wenthold RJ. Organization of NMDA receptors at extrasynaptic locations. Neuroscience. 2010; 167:68–87. [PubMed: 20096331]

Remy S, Csicsvari J, Beck H. Activity-dependent control of neuronal output by local and global dendritic spike attenuation. Neuron. 2009; 61:906–916. [PubMed: 19323999]

Rhodes KJ, Carroll KI, Sung MA, Doliveira LC, Monaghan MM, Burke SL, Strassle BW, Buchwalder L, Menegola M, Cao J, et al. KChIPs and Kv4 alpha subunits as integral components of A-type potassium channels in mammalian brain. J Neurosci. 2004; 24:7903–7915. [PubMed: 15356203]

Rhodes KJ, Keilbaugh SA, Barrezueta NX, Lopez KL, Trimmer JS. Association and colocalization of K+ channel alpha- and beta-subunit polypeptides in rat brain. J Neurosci. 1995; 15:5360–5371. [PubMed: 7623158]

Seikel E, Trimmer JS. Convergent modulation of Kv4.2 channel alpha subunits by structurally distinct DPPX and KChIP auxiliary subunits. Biochemistry. 2009; 48:5721–5730. [PubMed: 19441798]

Serodio P, Rudy B. Differential expression of Kv4 K+ channel subunits mediating subthreshold transient K+ (A-type) currents in rat brain. J Neurophysiol. 1998; 79:1081–1091. [PubMed: 9463463]

Shah MM, Hammond RS, Hoffman DA. Dendritic ion channel trafficking and plasticity. Trends Neurosci. 2010

Spruston N. Pyramidal neurons: dendritic structure and synaptic integration. Nat Rev Neurosci. 2008; 9:206–221. [PubMed: 18270515]

Spruston N, Schiller Y, Stuart G, Sakmann B. Activity-dependent action potential invasion and calcium influx into hippocampal CA1 dendrites. Science. 1995; 268:297–300. [PubMed: 7716524]

van Es MA, van Vught PW, Blauw HM, Franke L, Saris CG, Van den Bosch L, de Jong SW, de Jong V, Baas F, van't Slot R, et al. Genetic variation in DPP6 is associated with susceptibility to amyotrophic lateral sclerosis. Nat Genet. 2008; 40:29–31. [PubMed: 18084291]

Yuan LL, Adams JP, Swank M, Sweatt JD, Johnston D. Protein kinase modulation of dendritic K+ channels in hippocampus involves a mitogen-activated protein kinase pathway. J Neurosci. 2002; 22:4860–4868. [PubMed: 12077183]

Zagha E, Lang EJ, Rudy B. Kv3.3 channels at the Purkinje cell soma are necessary for generation of the classical complex spike waveform. J Neurosci. 2008; 28:1291–1300. [PubMed: 18256249]

Zagha E, Ozaita A, Chang SY, Nadal MS, Lin U, Saganich MJ, McCormack T, Akinsanya KO, Qi SY, Rudy B. DPP10 modulates Kv4-mediated A-type potassium channels. J Biol Chem. 2005; 280:18853–18861. [PubMed: 15671030]

Zhao C, Wang L, Netoff T, Yuan LL. Dendritic mechanisms controlling the threshold and timing requirement of synaptic plasticity. Hippocampus. 2010

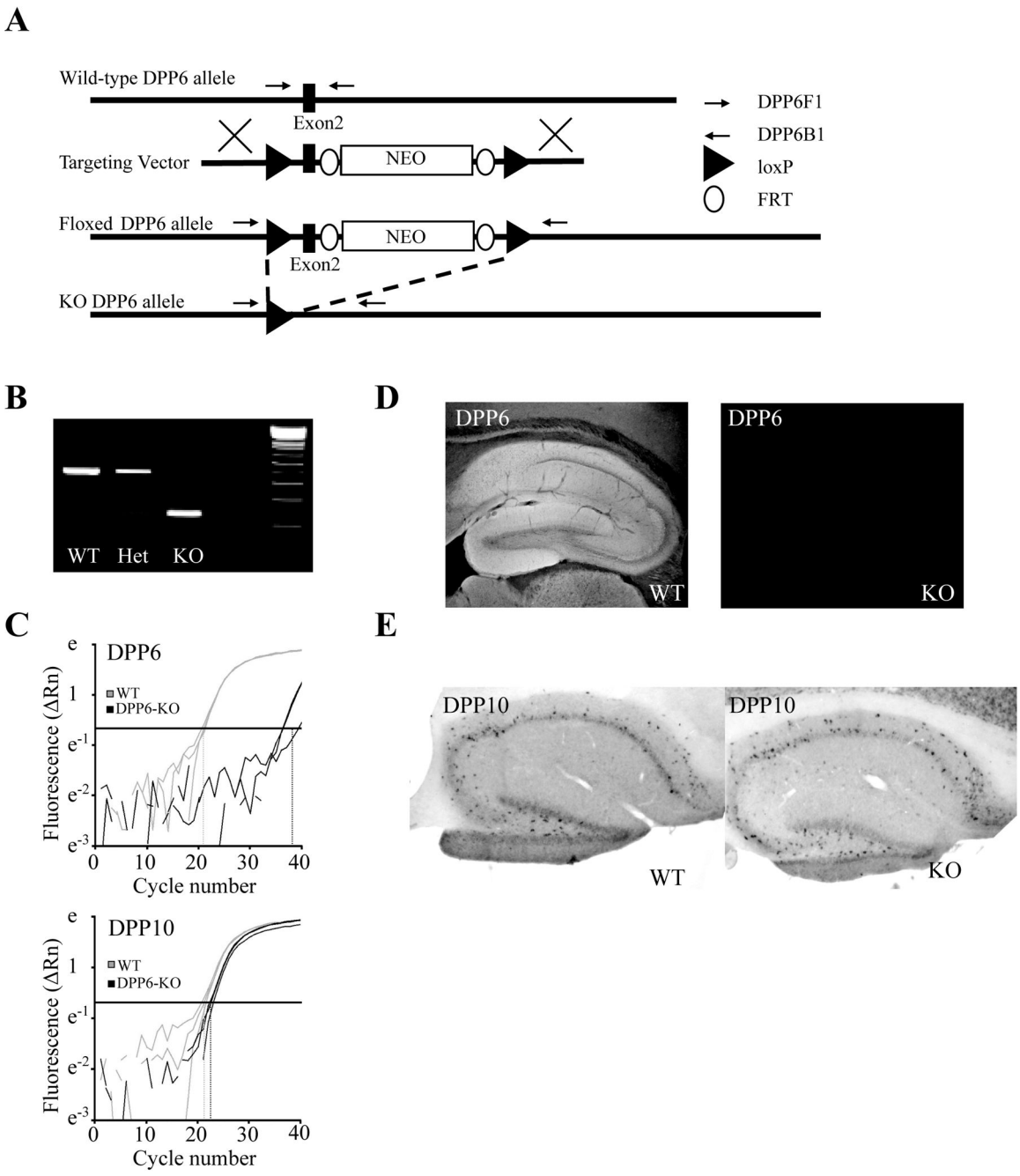

Figure 1. Construction and characterization of DPP6-KO mice

Targeted deletion of DPP6 exon 2 produces loss of DPP6 RNA and protein without producing compensatory changes in DPP10 expression. **(A)** A schematic describing the strategy used to delete a region of genomic DNA containing the second exon of DPP6. A targeting vector was 'knocked in' to the DPP6 locus via homologous recombination. Resulting mice were then crossed with mice expressing Cre-recombinase in germline cells causing recombination between the loxP sites flanking exon 2 and loss of the intervening genomic sequence. **(B)** PCR amplification product from a WT mouse, a mouse heterozygous for DPP6 deletion and a DPP6-KO mouse using primers DPP6F1 and DPP6B1 indicated in the schematic above. **(C)** Quantitative PCR amplification of DPP6 mRNA and mRNA from

the homologous gene DPP10 showing loss of DPP6 amplification product in the DPP6-KO (WT, Ct=20.9 ± 0.3; KO, Ct=37.3 ± 1.7) and no change in the amount of DPP10 product in the DPP6-KO (WT, Ct=22.7 ± 0.4; KO, Ct=21.5 ± 0.7). All qPCR experiments were performed with whole brain mRNA. **(D)** Loss of DPP6 immunoreactivity in the DPP6-KO. **(E)** Retained pattern of DPP10 in situ hybridization in the DPP6-KO.

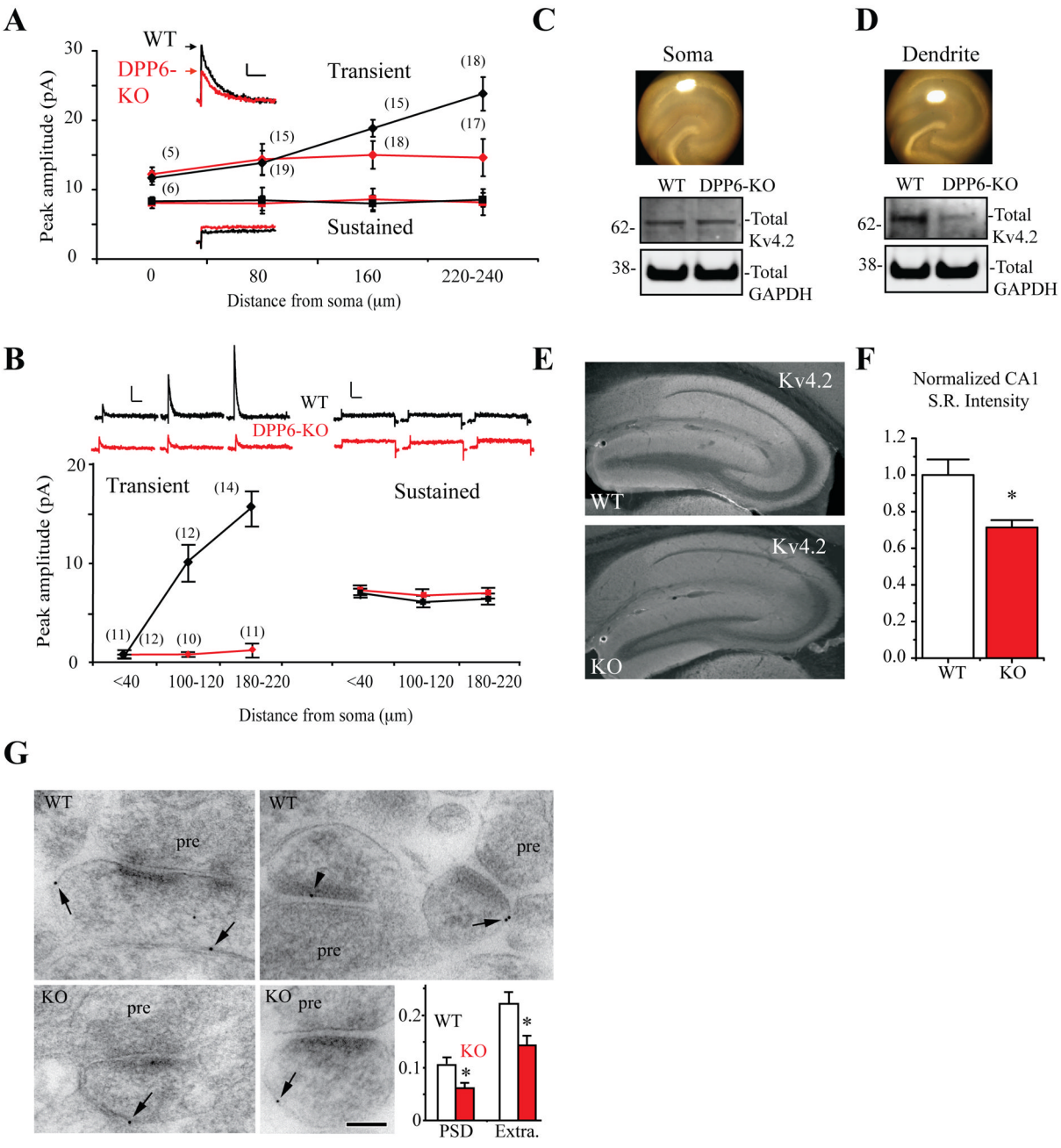

Figure 2. A-type K^+ current density gradient is abolished in DPP6-KO CA1 dendrites

(A) *Inset traces*. Representative current traces for both transient and sustained components of the total outward current recorded in outside-out patches pulled from CA1 pyramidal neuron dendrites (~240 μm from the soma) in acute hippocampal slices from both WT (black) and DPP6-KO mice (red). The transient component of total outward current (black diamonds) increases with distance from the soma in WT. However, in recordings from DPP6-KO mice, transient current amplitude (red diamonds) is constant throughout the dendrite. No difference in average sustained current amplitude was found between the two groups (WT, black squares; DPP6-KO red squares). Scale bars: 10 pA, 50 ms. Numbers in parentheses indicate number of patches. **(B)** Cell-attached recordings from CA1 dendrites of

WT and DPP6-KO mice confirmed increased A-current amplitude in DPP6-KO mouse dendrites. *Inset traces*. Representative current traces for both transient and sustained components of the total outward current recorded in cell-attached patches pulled from CA1 pyramidal neuron dendrites in acute hippocampal slices from both WT (black) and DPP6-KO mice (red). Multiple-fold increases over somatic average patch amplitude were found in WT distal dendrites (black diamonds) but not in recordings from DPP6-KO mice (red diamonds). Scale bars: 2 pA, 100 ms. No change in average sustained current amplitude was found between the two groups (WT, black squares; DPP6-KO red squares). Scale bars: 20 pA, 100 ms. Numbers in parentheses indicate number of patches. **(C,D)** Western blot results show that total Kv4.2 protein expression level is equivalent in the somatic area of WT and DPP6-KO slices but significantly reduced in the distal dendrites of DPP6-KO slices compared to WT (n=3, p<0.01). Images show hippocampal slices demonstrating somatic and dendritic punch areas. Excised tissue was used for western blot analyses. GAPDH served as a loading control. **(E)** Kv4.2 immunohistochemical labeling is reduced in the DPP6-KO. Images show mouse anti-Kv4.2 immunoreactivity in sagittal hippocampal sections from WT control and DPP6-KO mice. **(F)** Reduced immunofluorescence is quantified as average pixel intensity from rectangular fields placed throughout CA1 stratum radiatum (WT and DPP6-KO both n=21 fields from 3 mice each). **(G)** Immunogold localization of Kv4.2 in the CA1 stratum radiatum of the hippocampus of WT and KO mice. pre, presynaptic terminal; PSD, postsynaptic membrane/density; Extra, extrasynaptic membrane of the postsynaptic spine. Arrows show extrasynaptic labeling and arrowhead shows PSD labeling. Inset: pooled data from a total of 646 WT and 642 KO spine profiles showing reduced Kv4.2 in DPP6-KO PSD and extrasynaptic membrane. Asterisks denote p<0.05. Scale bar is 100 nm.

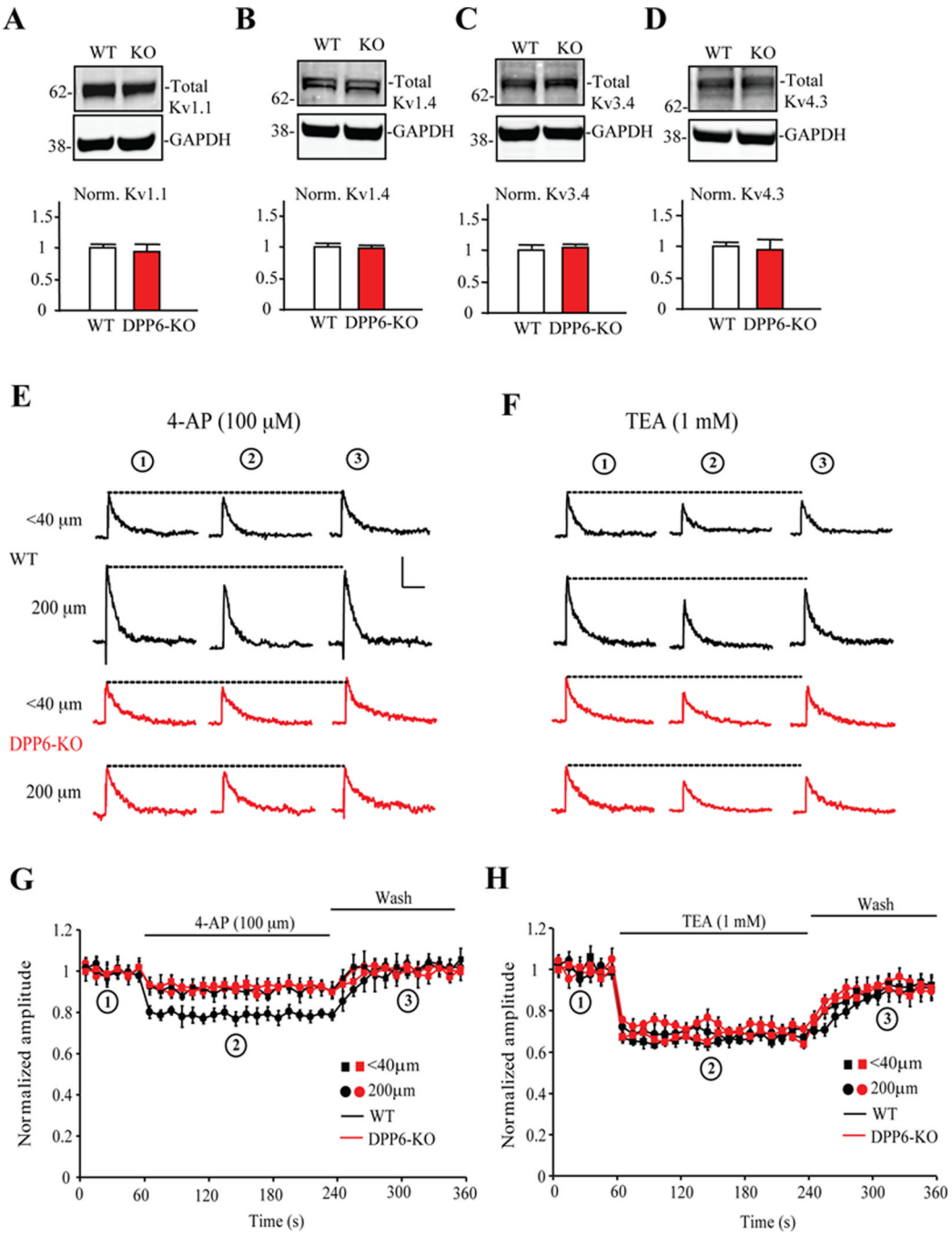

Figure 3. The A-type K^+ channels remaining in DPP6-KO dendrites are Kv4-mediated

(**A–D**) No significant differences in total protein expression of Kv1.1, Kv1.4, Kv3.4 or Kv4.3 were found between WT and DPP6-KO mice hippocampal slices. The separated proteins were immunoblotted using Kv1.1 (1:1000, NeuroMab), Kv1.4 (1:1000, NeuroMab), Kv3.4 (1:1000, NeuroMab), Kv4.3 (1:1000, NeuroMab) and GAPDH (1: 5000, Calbiochem) antibodies and visualized by Alexa Fluor 680 secondary antibody (1:10,000, Invitrogen) and Alexa Fluor 800 secondary antibody (1:10,000, Rockland). Pooled data were normalized to total GAPDH protein level. Error bars represent S.E.M. (n=4; p>0.05). (**E, F**) Example traces of A-currents recorded in outside-out patches pulled from proximal (<40 µm) and distal (200 µm) dendritic locations in WT (black) and DPP6-KO (red) before

(circle 1, at 30 seconds), during (circle 2, at 150s) and after (circle 3, at 320s) 100 μM low concentration 4-AP treatment **(E)** and 1mM TEA treatment **(F)**. Scale bars: 10 pA, 50ms. (**G,H**) Normalized A-current amplitude time course showing the effects of 100 μM 4-AP and 1mM TEA. 4-AP blocked a larger portion of the A-type K^+ current in WT distal dendritic (200 μm) recordings (n=14, p<0.05), but results did not differ between experimental groups treated with TEA (p>0.1). Together these results show no compensatory expression of Kv channels in DPP6-KO hippocampus.

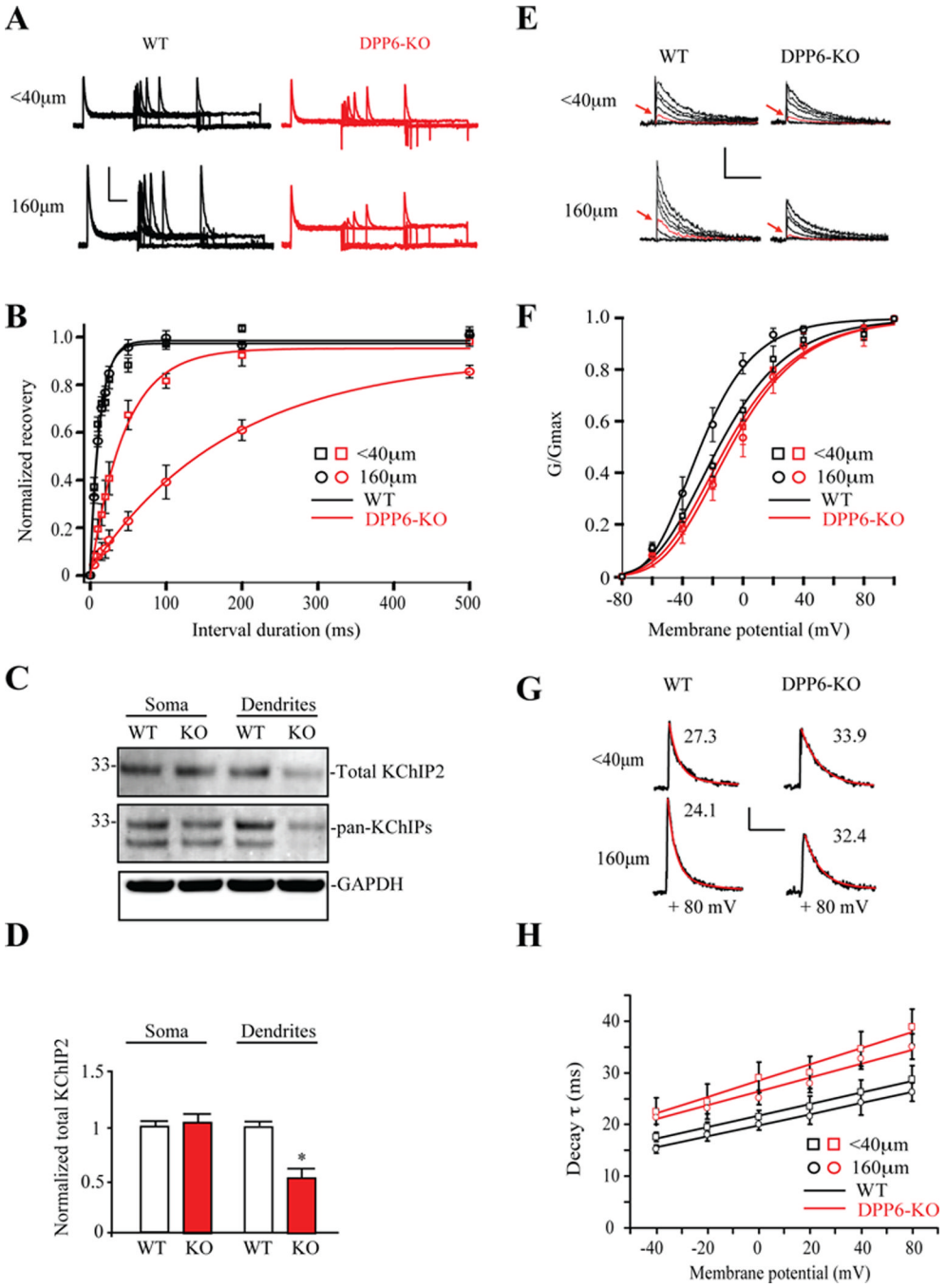

Figure 4. Properties of Kv4 channels remaining in DPP6-KO dendrites

(A) Example of A-current recovery traces from proximal and distal dendritic locations in WT and DPP6-KO mice. Recovery is noticeably slower than WT in DPP6-KO distal dendritic recordings. Scale bars: 10 pA, 200 ms. (B) Normalized recovery curves from DPP6-KO mice (n=8 for <40μm, n=9 for 160μm) shows considerably slower recovery than that from WT in distal dendritic but not proximal recordings (n=6 for <40μm, n=10 for 160μm). These results suggest that DPP6 is the primary regulator of recovery in WT dendrites. **(C)** KChIP2 expression is reduced in the distal dendrites of DPP6-KO slices compared to WT. Separated proteins were immunoblotted using KChIP1 (1:1000, NeuroMab, data not shown), KChIP2 (1:500, NeuroMab), KChIP3 (1:1000, NeuroMab, data

not shown), Pan-KChIP (1:1000, NeuroMab) and GAPDH (1: 5000, Calbiochem) antibodies. Total KChIP2 protein expression level is equivalent in the somatic area of WT and DPP6-KO tissue but significantly decreased in the distal dendrites of DPP6-KO compared to WT (n=3, p<0.01). **(D)** Pooled data normalized to total GAPDH protein level. Error bars represent S.E.M. **(E)** Example traces of dendritic A-currents used to produce activation curves in WT and DPP6-KO mice. Scale bars: 10 pA, 30 ms. Note the large difference in current amplitude at −20 mV (red trace in each set) between proximal (<40 μm) and more distal (160 μm) locations in WT, which is not evident in DPP6-KO recordings. **(F)** Activation curves produced from transient K^+ currents recorded at proximal (<40 μm, squares) and more distal dendritic (160 μm, circles) locations. A large (12 mV) leftward shift of activation curve was found in WT recordings ($V_{1/2}$=−16 mV, k=20, n=8 for <40μm, $V_{1/2}$=−28 mV, k=17. n=10 for 160μm). However, no shift was observed in DPP6-KO mice between proximal ($V_{1/2}$=− 11 mV, k=21, n=10) and distal dendritic ($V_{1/2}$=−8 mV, k=22, n=10) locations. The leftward shift in activation curve in WT recordings indicates an increase in the impact of A-type K^+ currents in dendrites. **(G)** DPP6 accelerates A-channel inactivation. Traces recorded in outside-out patches pulled from CA1 dendrites of WT and DPP6-KO mice. Red lines are fits to measure inactivation time constants (numbers above traces). Scale bars: 5 pA, 50 ms. **(H)** In both WT (n=8 and 10 for proximal and distal, respectively.) and DPP6-KO recordings (n=10 for both proximal and distal), inactivation rate increased with membrane potential. At all potentials, however, inactivation proceeded slower in mice lacking DPP6.

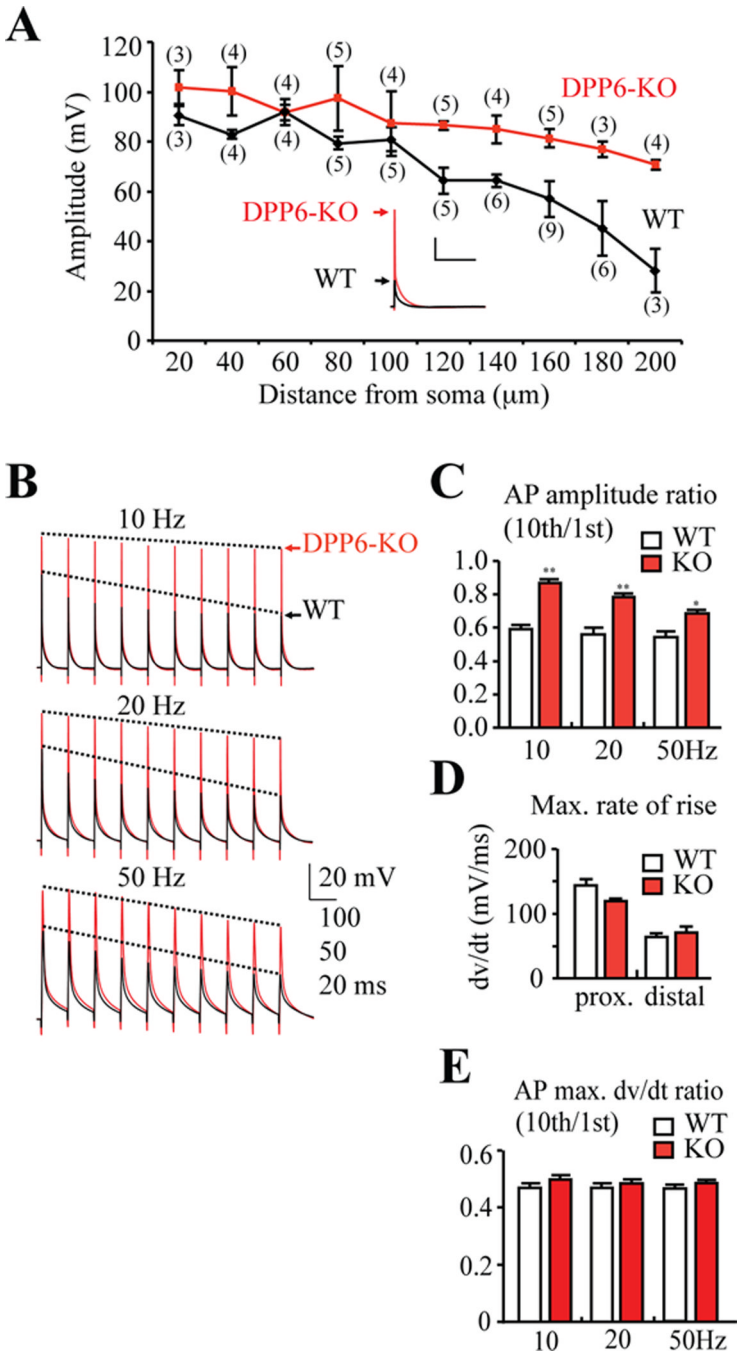

Figure 5. Enhanced dendritic excitability in DPP6-KO CA1 pyramidal neurons

(A) Back-propagating action potentials recorded in distal CA1 DPP6-KO dendrites (red) were larger in amplitude than those recorded in dendrites from WT mice (black). In WT recordings, bAP amplitude decreased with distance from the soma. Although bAP amplitude also slightly decreased in DPP6-KO recordings, significant differences in bAP amplitude from WT began at distances more than 100 μm from soma. *Inset*. Example bAP traces recorded from 180 μm distal dendrite. (#) Indicates number of patches. Scale bars: 20mV, 200 ms. **(B)** Example traces of AP trains elicited with 10, 20, and 50 Hz antidromic stimulation. All recordings were made ~160 μm from soma. **(C)** Pooled data shows that bAP amplitude exhibits a relatively small activity-dependent decrease in DPP6-KO (*n*=6 for 10,

20 and 50Hz) recordings compared to the much larger reduction in WT (*n*=6 for 10, 20 and 50Hz, $p<0.05$). **(D)** Although bAPs propagated better in DPP6-KO (*n*=7 for proximal, *n*=8 for distal) vs. WT (*n*=8 for proximal, *n*=13 for distal) recordings, no significant changes in the maximal rate of rise (an estimate of Na^+ channel activity) were found. **(E)** Maximal dv/dt ratio of 10^{th} to 1^{st} APs were equivalent between WT and DPP6-KO mice at all frequencies.

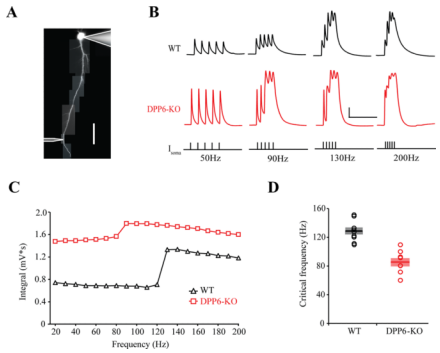

Figure 6. Calcium electrogenesis is enhanced in DPP6-KO CA1 dendrites

(A) Image demonstrating a dual somatic/dendritic recording. Scale bars: 40 μm. **(B)** Example traces of back-propagating AP trains elicited with 50, 90, 130 and 200 Hz with somatic current injection (I_{soma}). All recordings were made 200–220 μm from soma. Scale bars: 20mV, 100 ms. **(C)** Integral of membrane depolarization for a representative WT and DPP6-KO recording. The critical frequency is evident in the abrupt increase in depolarization around 90 Hz and 130 Hz in the DPP6-KO and WT recordings, respectively. **(D)** Pooled data shows that the critical frequency occurs at lower frequencies in the more excitable DPP6-KO dendrites. Solid line is the mean. Shaded area indicates S.E.M.

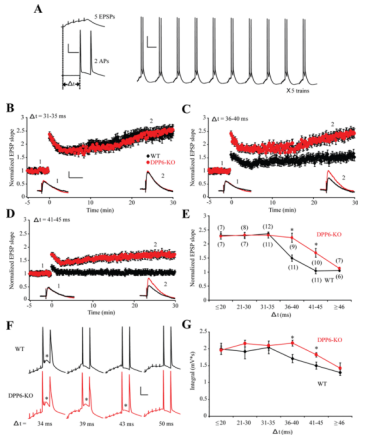

Figure 7. Spike-timing window for LTP induction is extended in DPP6-KO mice

(A) Theta burst pairing protocol (TBP) for LTP induction. Right: a representative response evoked by one train of LTP induction protocol. Each train contained 10 bursts of synaptic stimuli at 5 Hz with somatic current injections. The train was repeated 5 times. Scale bars: 20mV, 100ms. Left: Example traces of one burst. Each burst was composed of 5 EPSPs at 100 Hz and 2 action potentials at 50 Hz that were paired at various time windows (Δ t). Scale bars: 20mV, 20ms. (B–D) Magnitude of potentiation evoked by different time window stimulation protocols in WT and DPP6-KO mice. 31–35 time window (B) successfully boosted the magnitude of LTP to an equivalent level in both WT and DPP6-KO mice. Likewise, an extended time window from 35 ms to 45 ms (C,D) remained effective for LTP induction in DPP6-KO mice. However, the significant increase of EPSP slope can not be achieved in WT mice with a time window longer than 35ms. *Inset*. Example EPSP traces recorded before (number 1, −2min) and after (number 2, 25min) TBP from WT (black) and DPP6-KO mice (red). Scale bars: 2mV, 50ms. (E) LTP magnitude – timing plot revealed that an expanded time window for LTP induction exists in DPP6-KO mice. (#) Indicates number of patches. * indicates $p<0.05$. (F) Example traces evoked by single burst of TBP protocol with 34ms, 39ms, 43 ms and 50ms time window. * indicates putative calcium spikes. Scale bars: 20mV, 20ms. (G) Average integral of membrane depolarization for WT and DPP6-KO recordings at various time windows. Note a larger integral was accompanied by an increase of LTP magnitude. Compared with WT, DPP6-KO mice exhibited relatively larger single burst integral between 36–45 ms time window indicates an extension of spike-timing window of LTP induction. * indicates $p<0.05$.

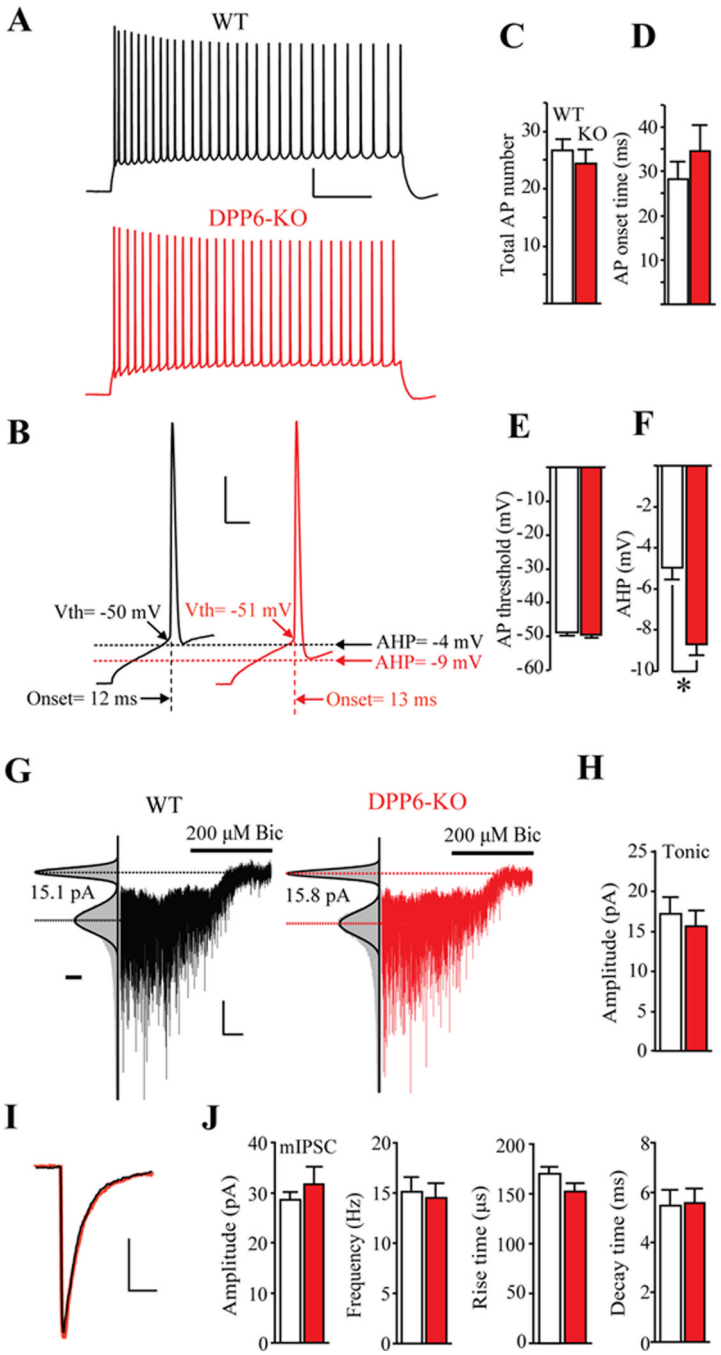

Figure 8. Somatic membrane excitability and GABAergic currents are unaffected in DPP6-KO CA1 neurons

(A) Traces in response to a 1000 ms, 200 pA somatic current injection in WT (black trace) and DPP6-KO (red trace) CA1 hippocampal neurons. Scale bar: 20 mV, 100 ms. **(B)** Expanded traces from (A) to more clearly depict AP onset time, threshold and AHP. Scale bar: 20 mV, 5 ms. **(C)** The number of APs recorded from hippocampal CA1 neurons over the course of 1 sec for a 200 pA current injection. No differences were found between WT (n=24) and DPP6-KO mice (n=23, p>0.1). **(D, E, F)** Pooled data showing 1st AP AHP, onset time and threshold potential, respectively, for CA1 pyramidal neurons. Compared with WT (n=24), a significant difference was found only for AHP in DPP6-KO (n=23, p<0.05). **(G)**

Example whole-cell recorded traces from WT (black) and DPP6-KO (red) CA1 neurons show a holding current difference before and after bicuculline (200 μM) treatment. Left panel: Gaussian fits to all-points histograms derived from a 20s recording periods before or after application of bicuculline. The difference between the Gaussian means marks by the dotted lines indicates the tonic GABA currents. Scale bar below the fit curve represent the number of counts in 1 pA bins and is equal to 4000 counts. Scale bars: 10 pA, 20 s. **(H)** Group data of tonic current blocked by bicuculline. **(I)** Average mIPSC traces from 435 events for WT (black trace) and 486 events for DPP6-KO (red trace). Scale bars: 10 pA, 10 ms. **(J)** Group data of mIPSC of (from left to right): amplitude, frequency, rise time and decay time. No differences were found between WT (n=12) and DPP6-KO (n=13) recordings (p>0.1).